Ultralow Pt-loading bimetallic nanoflowers: fabrication and sensing applications

2013 Nanotechnology 24 025501

(http://iopscience.iop.org/0957-4484/24/2/025501)

Nanotechnology **24** (2013) 025501 (9pp) doi:10.1088/0957-4484/24/2/025501

Ultralow Pt-loading bimetallic nanoflowers: fabrication and sensing applications

Qingqing Wu[1], Yongxin Li[1,2], Hongying Xian[1], Chaodi Xu[1], Lun Wang[1] and Zhibing Chen[3]

[1] College of Chemistry and Materials Science, Anhui Normal University, Wuhu 241000, People's Republic of China
[2] Corrosion and Sustainable Infrastructure Lab, Western Transportation Institute, Montana State University, PO Box 174250, Bozeman, MT 59717-4250, USA
[3] Department of Chemistry–Biology, Suzhou University, Suzhou, Anhui 234000, People's Republic of China

E-mail: yongli@mail.ahnu.edu.cn and yongxin.li@coe.montana.edu

Received 2 August 2012, in final form 26 October 2012
Published 10 December 2012
Online at stacks.iop.org/Nano/24/025501

Abstract
Ultralow Pt-loading Au nanoflowers (AuNFs) were synthesized on a glassy carbon electrode surface by the underpotential deposition (UPD) monolayer redox replacement technique, which involves redox replacement of a copper UPD monolayer by $PtCl_4^{2-}$ that can be reduced and deposited simultaneously. Field-emission scanning electron microscopy, energy dispersive spectroscopy, x-ray photoelectron spectroscopy and the electrochemical method were utilized to characterize the ultralow Pt-loading AuNFs. Cyclic voltammogram results showed that the ultralow Pt-loading AuNFs exhibited excellent electrocatalytic activity towards the reduction of hydrogen peroxide and the oxidation of glucose in neutral media, and the reaction pathway of glucose oxidation was changed from an intermediate process based on the electrosorption of glucose to a direct oxidation process. From chronoamperometric results, it could be obtained that this prepared biosensor had wide linear ranges and very low detection limits (DLs) for H_2O_2 (0.025–94.3 μM; DL = 0.006 μM) and glucose (0.0028–8.0 mM; DL = 0.8 μM), which were much better than previous results.

S Online supplementary data available from stacks.iop.org/Nano/24/025501/mmedia

(Some figures may appear in colour only in the online journal)

1. Introduction

Electrochemical biosensors utilizing nanomaterials have recently attracted considerable attention in the area of sensing [1–3]. Many kinds of nanomaterials, such as carbon nanotubes [4, 5], gold and platinum nanoparticles [6], and semiconductors [7], have been used in biosensors in the environmental science, medicine and food quality control field. In particular, because of their usefulness in the diagnostic analysis of diabetes, glucose biosensors based on nanomaterials, such as carbon nanotubes and metal nanoparticles, have been extensively studied in recent years [1, 4–6, 8–14]. Bimetallic nanoparticle assemblies, such as Pt, Au and Pd based bimetallic systems, are of particular importance in catalysis and sensing because they show many favorable properties in comparison with the corresponding monometallic part [4, 5, 13, 15, 16]. Because catalysis and sensing reactions are extremely sensitive to the atomic-level details of the surface properties, deliberate tailoring of the surface nanostructure of the catalysts is an interesting target and could lead to the exploitation of novel catalysts with unique properties [17]. Unfortunately, most of the bimetallic catalysts used in catalysis and sensing fields are prepared by mixing the two metal parts together through

electrodeposition, self-assembly, and other techniques [5, 13, 14, 18]. In recent years, the underpotential deposition (UPD) monolayer redox replacement technique, which involves redox replacement of an underpotential deposition monolayer by more noble metal cations that can be reduced and deposited simultaneously, has been utilized to prepare bimetallic nanoparticles with core@shell structures [19–25]. For example, Adzic and co-workers [19–22, 25] have reported the electrocatalytic activity of core@shell nanoparticles prepared by UPD of a sacrificial metal onto the core, followed by galvanic exchange. Brankovic *et al* [26–29] have carefully investigated the kinetics and some important issues (size dependence, electrolytes, etc) of the surface-limited redox replacement reaction (SLRR) through *in situ* scanning tunneling microscopy (STM), density functional theory (DFT) and the electrochemical method. Dimitrov [30–32] and Stickney [33–35] have also made contributions to kinetics research via SLRR. Crooks *et al* [23, 24, 36] have developed the UPD/galvanic exchange process for synthesis of Au@Pt dendrimer-encapsulated nanoparticles on a glassy carbon surface. A similar approach was used to synthesize Pt monolayer shells on Au nanoparticles by Dong *et al* [17]. Up to now, all the bimetallic nanoparticles prepared by the UPD monolayer redox replacement technique have been utilized to investigate catalytic properties in fuel cells, such as oxygen reduction, methanol and formic acid oxidation, and no reports have been found of their use in the sensing field, although theoretical calculation [37–39] shows that these ultrathin metal-coated bimetals are sensitive to some species such as hydrogen peroxide.

On the other hand, the development of sensing devices with high performance is very important for the diagnosis of diabetes mellitus and the detection of hydrogen peroxide, topics of worldwide public health and environmental concern. Electrochemical glucose and hydrogen peroxide biosensors have been developed widely due to their simple, accurate and quick response and fast analytical process [1, 4–6, 8–13, 40–42]. Among them, direct electrocatalytic oxidation of glucose or reduction of hydrogen peroxide at a nonenzymatic electrode exhibits convenience and advantages in avoiding the drawbacks of enzymatic sensors. Many nonenzymatic glucose/hydrogen peroxide sensors, especially Pt-based amperometric glucose/hydrogen peroxide sensors, have been fabricated [1, 3, 5, 8–11, 43, 44]. Unfortunately, many problems for the application of sensors, such as low sensitivity, poor stability and interference, still exist. The development of novel nonenzymatic glucose/hydrogen peroxide sensors with low detection limit, good stability and selectivity, and quick response is a challenge even now.

In this paper, we report a new approach to prepare ultralow Pt-loading Au flower-like nanostructures (AuNFs) using a Cu UPD process, followed by the *in situ* redox replacement reaction of the Cu monolayer by Pt. Electrochemical results demonstrate that this ultralow Pt-loading AuNFs exhibit excellent electrocatalytic activity towards the reduction of hydrogen peroxide and glucose oxidation with good reproducibility and selectivity, a low detection limit and a wide linear range, which can potentially be utilized as a novel biosensor to analyze real samples. More interestingly, from the cyclic voltammogram of glucose using an ultralow Pt-loading AuNFs modified electrode, glucose can be directly oxidized and does not need the intermediate process that has been reported extensively.

2. Experimental section

Chemicals. $HAuC1_4{\cdot}4H_2O$ (Au% > 48%), $K_2PtCl_4{\cdot}6H_2O$ (Pt% > 40%), hydrogen peroxide (30% w/v solution), β-D(+)-glucose and potassium ferricyanide ($K_3Fe(CN)_6$) were obtained from Sigma-Aldrich. Choline chloride (Ch), $HClO_4$, KCl and $Cu(NO_3)_2$ were purchased from Shanghai Chemical Co., Ltd (Shanghai, China). All reagents used were of analytical grade. The 0.1 M phosphate buffer solutions (PBS) with different pH values were prepared by mixing four stock solutions of H_3PO_4, KH_2PO_4, K_2HPO_4 and KOH provided by Shanghai Chemical Co., Ltd (Shanghai, China). All aqueous solutions were prepared in doubly distilled, deionized water. High purity nitrogen was used for deaeration.
Apparatus. The electrochemical experiments, including cyclic voltammetry (CV), chronoamperometry and electrochemical impedance spectroscopy (EIS), were performed on a CHI 660C electrochemical workstation (ChenHua, Shanghai, China). Field-emission scanning electron microscopy (FE-SEM) images were obtained using a JSM-6700F mode microscope (JEOL, Japan). X-ray photoelectron spectroscopy (XPS) measurement was performed on an ESCALAB-MKII spectrometer (VG Co., UK) with a Mak-Alpha radiation source (x-ray radiation as the x-ray source for excitation and an analyzer pass energy of 50 eV).

All experiments were carried out with a three-electrode system consisting of an Ag/AgCl reference electrode, a Pt foil auxiliary electrode and a glass carbon disk electrode (GCE, ⌀ 3.0 mm) as a working electrode. A digital pH/mV meter (model 780 Metrohm, Jiangsu, China) was used for the preparation of the buffer solution. All experiments were carried out at room temperature.
Preparation of the modified electrode. The preparation procedure for the ultralow Pt-loading Au nanoflowers on the GCE surface is illustrated schematically in scheme 1. The GCE was polished with 1.0, 0.3 and 0.05 μm α-Al_2O_3 powder successively and sonicated in water for about 3 min after each polishing step. Finally, the electrode was sonicated in ethanol and distilled water for 5 min, and dried with a high purity nitrogen stream immediately before use.

A freshly polished GCE was immersed into 0.1 M PBS (pH 7.0) solution containing 2.0 mM Ch and 10 mM $LiClO_4$ by cyclic scanning in the range of −1.8–1.7 V for six cycles at a scan rate of 25 mV s^{-1}. The modified process is shown in figure S1 (see the supporting information available at stacks.iop.org/Nano/24/025501/mmedia). After the Ch modified GCE had been dried under purified nitrogen, a Ch monolayer was formed on the GCE surface due to the formation of a C–N bond [45–47]; this is denoted as Ch/GCE. Au nanoflowers (AuNFs) were formed on the Ch/GCE surface in a 0.2 mg ml^{-1} $HAuCl_4$ solution by the chronoamperometric method in the potential range

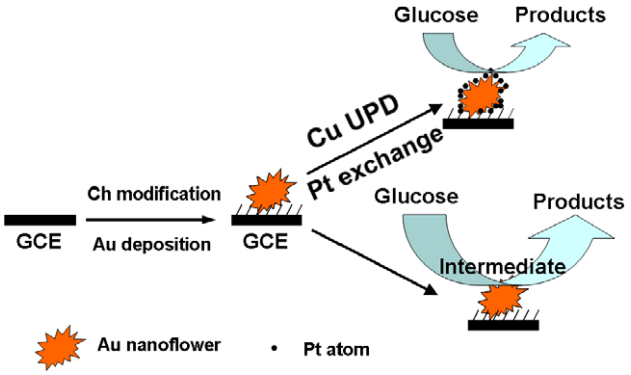

Scheme 1. The fabrication procedures for the ultralow Pt-loading AuNFs on a glassy carbon electrode surface and their electrocatalysis.

of −0.2–0 V for a deposition of 200 s (denoted as AuNFs/Ch/GCE) [48, 49]. Cu underpotential deposition (UPD) on the AuNFs/Ch/GCE surface was performed by holding the potential at 0.02 V in a 0.1 M $HClO_4$ solution containing 1.0 mM $Cu(NO_3)_2$ for 120 s; this is similar to our previous process [50] and other reports [19, 20, 22, 24, 36]. After rinsing with water and drying with a nitrogen stream, the modified electrode was transferred to a solution of 5.0 mM K_2PtCl_4 in deaerated 0.1 M $HClO_4$ for 15 min to ensure complete redox replacement of the UPD Cu, and a Pt monolayer coated AuNP modified electrode could be formed (denoted as Pt@AuNFs/Ch/GCE). This obtained electrode was rinsed with water and stored in a refrigerator (4 °C) for further use.

3. Results and discussion

3.1. Electrochemical design of the ultralow Pt-loading Au nanoflowers

AuNFs were electrodeposited on the Ch/GCE surface due to the radial diffusion of $AuCl_4^-$ ions on the Ch/GCE surface (see below). A typical CV of the AuNF modified electrode was obtained from −0.2 to 1.4 V (versus Ag/AgCl) in 0.5 M H_2SO_4 at a scan rate of 50 mV s^{-1} (as shown in figure 1(A), curve (a)). The presence of oxide at high anodic potentials (>1.3 V) and the cathodic removal of oxide at ∼0.92 V confirms the formation of AuNFs [24, 50]. A UPD copper monolayer was deposited on the AuNF surface by holding the potential at 0.02 V for 120 s in a 0.1 M $HClO_4$ solution containing 1.0 mM $Cu(NO_3)_2$. A typical CV was recorded for the AuNFs modified electrode in a deaerated 0.1 M $HClO_4$ solution containing 1.0 mM $Cu(NO_3)_2$, as shown in figure 1(B). It could be observed that four peaks appeared in figure 1(B). Peaks a and b refer to the formation of UPD copper and bulk copper, while peaks b′ and a′ correspond to the dissolution of bulk and UPD copper, respectively [17].

After deposition of a Cu monolayer on the surface of the AuNFs, the electrode was transferred to a solution of 0.10 M $HClO_4$ + 5.0 mM K_2PtCl_4 for 5 min and a galvanic exchange reaction took place, and a Pt monolayer was formed on the surface of the AuNFs. Curve (b) in figure 1(A) gives the CV of the ultralow Pt-loading AuNFs/Ch/GCE in a 0.5 M H_2SO_4 solution, in which the typical features of the Au electrochemistry are not observed, whereas the typical Pt features, including hydrogen adsorption and desorption at ∼−0.2–0 V, and the formation (>1.1 V) and removal of Pt oxide (∼0.46 V), demonstrate that a Pt monolayer has been formed on the surface of the AuNFs [17, 24, 50]. From the small peak at ∼0.92 V (figure 1(A), curve b), which is the typical Au peak of oxide reduction [17, 24, 50], it can be concluded that no alloying or severe agglomeration had occurred and a uniform ultralow Pt-loading AuNF core@shell nanostructure had been fabricated on the GCE surface.

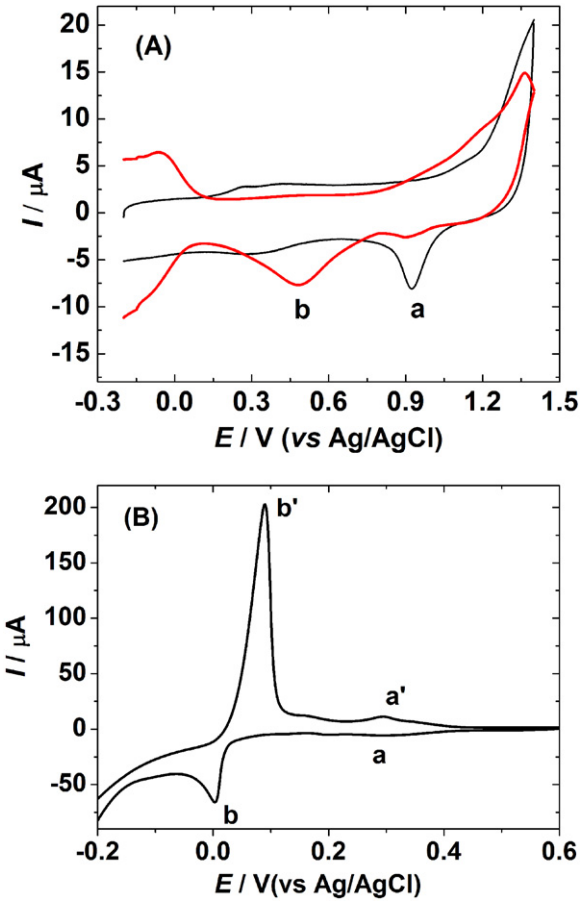

Figure 1. (A) CVs of AuNFs/Ch/GCE (a) and ultralow Pt-loading AuNFs/Ch/GCE (b) in N_2-saturated 0.5 M H_2SO_4. (B) CVs for AuNFs/Ch/GCE in 1 mM $Cu(NO_3)_2$ + 0.1 M $HClO_4$. Scan rate: 50 mV s^{-1}.

It is well known that the deposition potential and time are two important parameters in the UPD Cu process [50, 51]. Figure S2 (see the supporting information available at stacks.iop.org/Nano/24/025501/mmedia) shows a series of voltammetric responses of a AuNFs modified GCE after Cu UPD for different deposition potentials. It can be obtained that the oxidation charge from Cu UPD depends on the deposition potential. The calculated results showed that the amount of Cu oxidation charge was stable when the applied potential range was between 0.01 and 0.05 V, while when the deposition potential went outside this range, the calculated

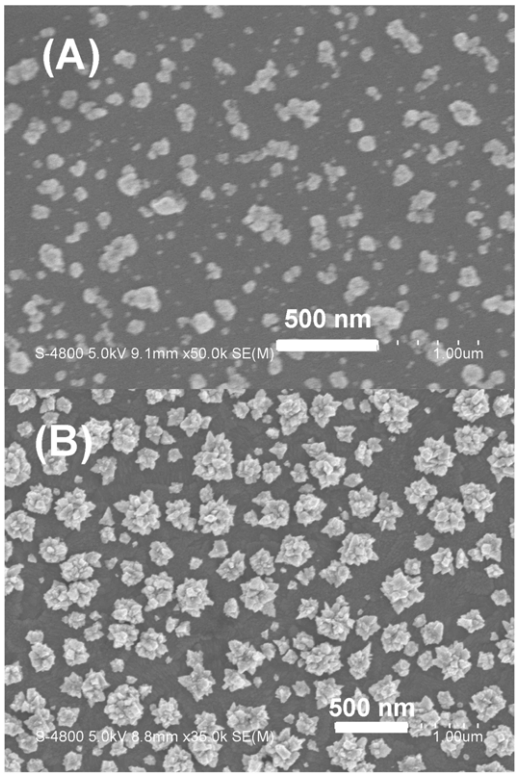

Figure 2. FE-SEM images of Au nanoparticles immobilized on the bare GCE surface (A), and Au nanoflowers immobilized on the Ch/GCE surface (B).

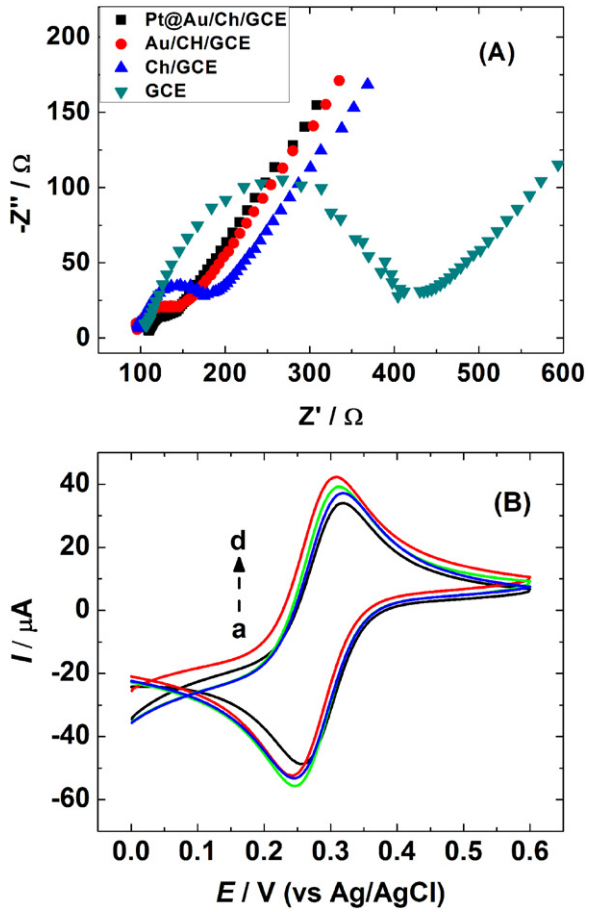

Figure 3. (A) Complex plane impedance plots in 10 mM $K_3[Fe(CN)_6]$:$K_4[Fe(CN)_6]$ (1:1) mixture containing 0.1 M KCl at the bare GCE (a), Ch/GCE (b) AuNFs/Ch/GCE (c) and Pt@Au/Ch/GCE (d), respectively. (B) CVs of 5.0 mM $K_3[Fe(CN)_6]$ + 0.1 M KCl at the bare GCE (a), Ch/GCE (b), AuNFs/Ch/GCE (c) and Pt@Au /Ch/GCE (d). Scan rate: 50 mV s^{-1}.

charge would become smaller. Therefore, 0.02 V was selected as the potential for Cu UPD in this study. Meanwhile, the Cu UPD time was investigated and figure S3 (see the supporting information available at stacks.iop.org/Nano/24/025501/mmedia) shows a series of voltammetric responses of the AuNFs modified GCE after Cu UPD for different time durations. From figure S3 (see the supporting information available at stacks.iop.org/Nano/24/025501/mmedia), it can be obtained that the Cu deposition at the Au surface takes ∼120 s to reach the saturated value, which is in agreement with our previous results [50].

3.2. Characterization of the ultralow Pt-loading Au nanoflowers

Field-emission scanning electron microscopy (FE-SEM) measurements were made to investigate the surface morphology and shape of the gold nanomaterial deposited on the GCE surface. Figure 2 shows the typical SEM images for electrodeposition on bare the GCE surface (A) and the Ch/GCE surface (B). It can be seen that a uniform Au nanoflower-like morphology with a diameter of ∼250 nm is formed on the Ch/GCE surface. However, only Au nanoparticles can be found on the bare GCE surface. It is well known that the electrodeposition can be controlled by three processes: mass transfer (diffusion and convection), the electrochemical reaction (or the electron transfer rate) and crystallization (nucleation and growth) [48, 52]. At the beginning, Au atoms will be produced on the surface of the substrate by the electrochemical reduction of $AuCl_4^-$, and then the Au nuclei will undergo crystal growth and form different shapes based on the surface properties of the substrate. For the Ch monolayer covered GCE, Au nuclei always form at the ends of Ch chains due to the electrostatic interaction between the positively charged Ch and the negatively charged $AuCl_4^-$ ions, and their growth always takes place at the same sites. Because the space between Ch molecules is relatively large and the diffusion of $AuCl_4^-$ on the Au nuclei surfaces is radial diffusion, a AuNF structure can be seen on the Ch/GCE surface (figure 2(B)), whereas the density of reaction active sites on the bare GCE is high and the diffusion of $AuCl_4^-$ on Au nuclei is three-dimensional, so Au nanoparticles can be observed on the bare GCE surface (figure 2(A)) [48, 53]. Moreover, the SEM image of ultralow Pt-loading AuNFs is similar to the AuNFs image, which means that the Pt layer is too thin to be seen (data not shown). Energy dispersive spectroscopy (EDS) was also used to characterize the modification process on the Ch/GCE surface and figure S4 (in the supporting information available at stacks.iop.org/Nano/24/025501/mmedia) gives the EDS

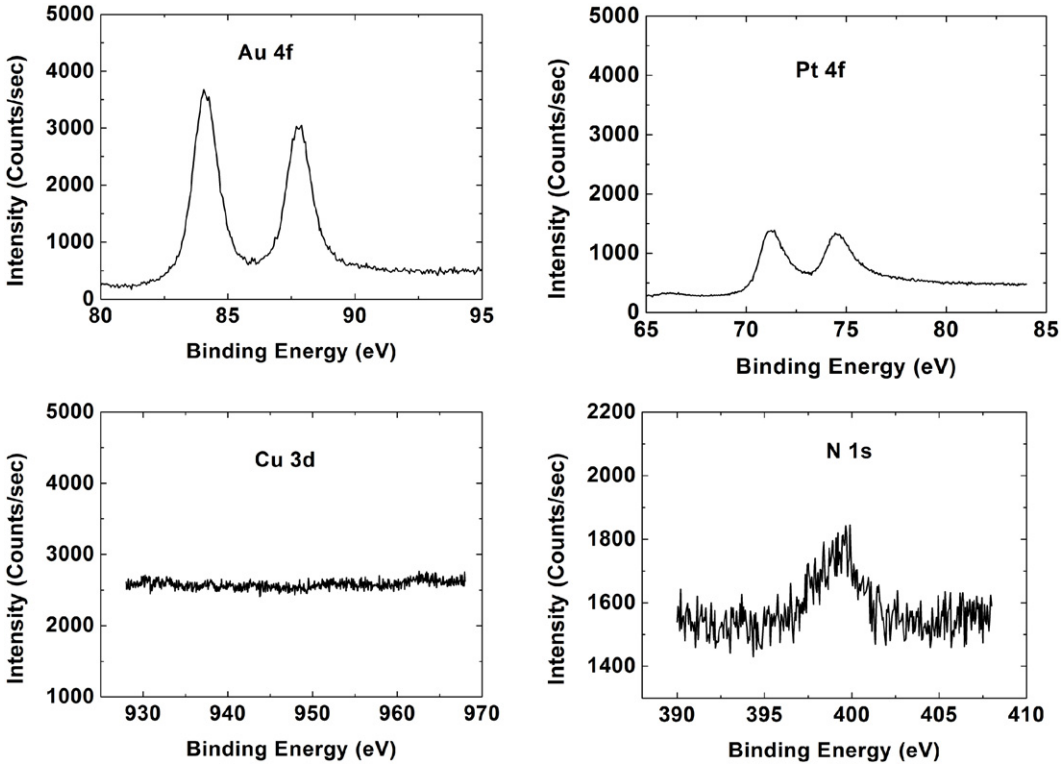

Figure 4. XPS spectra of ultralow Pt coated AuNFs modified on a Ch/GC surface.

results for AuNFs/Ch/GCE (A), Cu@AuNFs/Ch/GCE (B) and Pt@AuNFs/Ch/GCE (C). From the relative intensity of Cu/Au and Pt/Au, it could be concluded that ultrathin Cu layer was modified on the surface of the AuNFs and then replaced by the ultrathin Pt layer.

EIS is an effective method for probing the features of a surface-modified electrode using the redox probe $Fe(CN)_6^{3-}/Fe(CN)_6^{4-}$ [48, 49]. Figure 3(A) illustrates the results of impedance spectroscopy on the bare GCE (curve (a)), Ch/GCE e (curve (b)), AuNFs/Ch/GCE (curve (c)) and Pt@Au/Ch/GCE (curve (d)) in the presence of equivalent 10 mM $Fe(CN)_6^{3-/4-}$. The electro-transfer resistance (R_{et}) value can be directly measured as the diameter of the semicircle. As shown in figure 3(A), the R_{et} value for the modified electrode is decreased dramatically in comparison with the bare GCE, which should be ascribed to the good property of the Ch monolayer that forms a high electron conduction pathway between the electrode surface and the $Fe(CN)_6^{3-}/Fe(CN)_6^{4-}$ probe. This result also indicates that the Pt monolayer coated AuNFs and Ch layers are gradually immobilized on the surface of the GCE.

CVs were employed to investigate the electrochemical properties of the modified electrodes. As shown in figure 3(B), a pair of quasi-reversible redox peaks of $Fe(CN)_6^{3-}$ with a peak separation (ΔE_p) of 50 mV exists for the bare GCE (curve (a)). The peak currents increased slightly with the Ch/GCE (curve (b)), the AuNFs/Ch/GCE (curve (c)), and the Pt@Au/Ch/GCE (curve (d)) due to either the good conductivity of the Ch monolayer or the large surface area of the Pt monolayer coated AuNFs modified on the surfaces of the electrodes. These results are in agreement with the EIS data, indicating that the Ch monolayer and ultralow Pt-loading AuNFs have been immobilized on the GCE surface successfully.

XPS measurements were also performed to identify the ultralow Pt coated AuNFs on a glassy carbon chip, and high resolution scans of the Cu 3d, Au 4f, Pt 4f and N 1s regions are shown in figure 4. The Au $4f_{7/2}$ peak is located at a binding energy of 84.0 eV, which corresponds to zero-valent Au [54]. The Pt $4f_{7/2}$ peak is located at a binding energy of 71.2 eV, which corresponds to zero-valent Pt [54]. In the N(1) region, the N/C ratio (nitrogen to carbon) was increased to 167% and the peak shifted slightly from 400.20 to 399.8 eV after the modification, reflecting the existence of nitrogen containing residues on the GCE surfaces [55]. No obvious signal was observed from the Cu 3d region, indicating that the galvanic exchange was complete and the AuNFs surfaces were Cu-free.

3.3. Electrochemical performance of the ultralow Pt-loading AuNFs for H_2O_2 sensing

Figure 5 shows the typical CVs of 0.05 mM hydrogen peroxide at different electrodes. No response is observed for 0.05 mM H_2O_2 on the Ch/GCE (curve (a)), and the AuNFs/Ch/GCE gives a very weak response to H_2O_2 at quite a negative potential (∼−0.25 V, curve (b)), which is similar to previous results [56]. Although the bulk Pt coated AuNFs/Ch/GCE exhibits a more sensitive response (curve (c)), the ultralow Pt-loading AuNFs/Ch/GCE exhibits an excellent response signal, and the peak potential is ∼0.09 V. Compared with the bulk Pt coated AuNFs/Ch/GCE, it can be

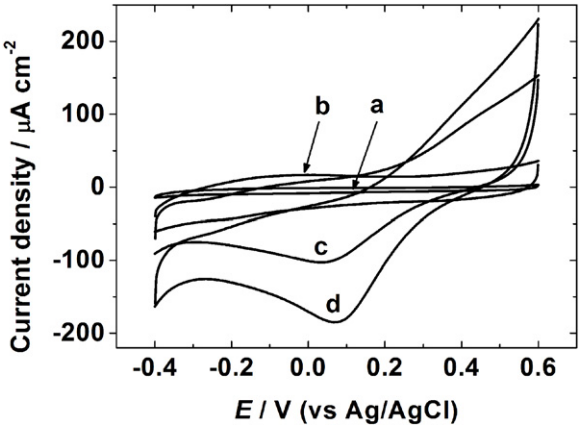

Figure 5. CV responses of 0.05 mM H_2O_2 in 0.1 M PBS (pH 7.0) at the bare GCE (a), AuNFs/Ch/GCE (b), bulk Pt coated AuNFs/Ch/GCE (c) and ultralow Pt-loading AuNFs/Ch/GCE (d). Scan rate: 50 mV s^{-1}.

deduced that the excellent electrocatalytic activity towards the reduction of H_2O_2 of the ultralow Pt-loading AuNFs/Ch/GCE is due to the Pt monolayer, which is in accordance with previous results [57].

The dependence of the electrochemical behavior of the ultralow Pt-loading AuNFs modified electrode on the pH was studied. CVs of the modified electrode in PBS at various pH values ranging from 5.0 to 9.0 are shown in figure S5 (see the supporting information available at stacks.iop.org/Nano/24/025501/mmedia). It is found that an increase of the pH in the solution leads to a negative shift in the potential of the cathodic peak for the modified electrode (see figure S5A in the supporting information available at stacks.iop.org/Nano/24/025501/mmedia). The relationship between E_{pc} and pH can be given by the following equation: $E_{pc}(V) = 0.513–0.064$ pH ($r = 0.9922$, see figure S5B in the supporting information available at stacks.iop.org/Nano/24/025501/mmedia), which means that the uptake of electrons is accompanied by an equal number of protons. Increase of the pH from 5.0 to 9.0 would lead to a slight increase of the peak current, whereas further increase of the pH beyond 7.0 would cause the peak current to decrease (see figure S5C in the supporting information available at stacks.iop.org/Nano/24/025501/mmedia). In this study, pH 7.0 PBS was chosen as the supporting electrolyte since it is close to the pH value of physiological conditions. CVs of 0.05 mM H_2O_2 in PBS (pH 7.0) using the ultralow Pt-loading AuNFs modified electrode at different scan rates were also recorded, as shown in figure S6 (see the supporting information available at stacks.iop.org/Nano/24/025501/mmedia). From figure S6 (available at stacks.iop.org/Nano/24/025501/mmedia), it can be seen that the cathodic peak current increases linearly with scan rate in the range of 50–350 mV s^{-1} (inset), indicating a surface-adsorption controlled process.

Considering the good electrocatalytic activity of the ultralow Pt-loading AuNFs/Ch/GCE towards the reduction of H_2O_2, the chronoamperometric method for the detection of H_2O_2 was attempted. Figure 6(A) shows the steady-state current responses of the Ch/GCE (curve (a)), AuNFs/Ch/GCE

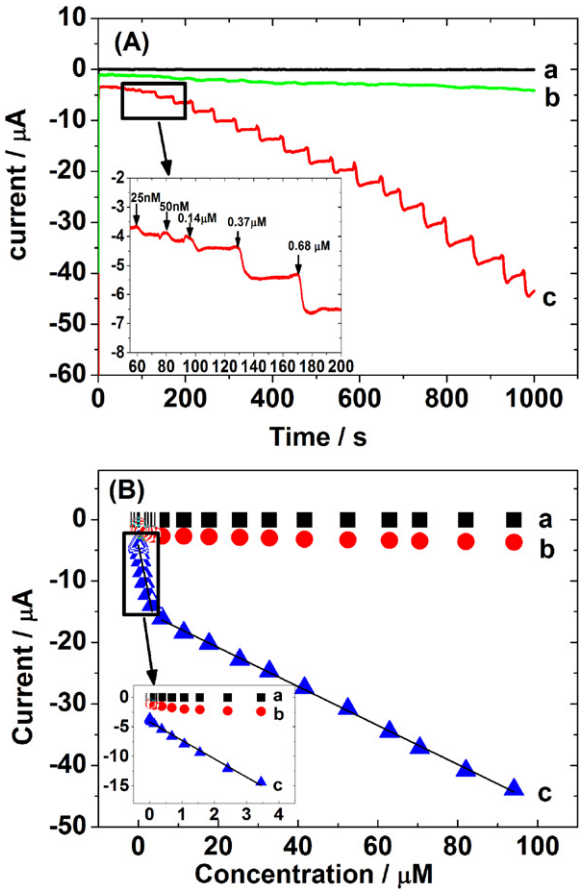

Figure 6. (A) Chronoamperometry response curves at an applied potential of 0.09 V with the injection of various concentrations of H_2O_2 into 5 ml of stirred PBS (pH 7.0) for the Ch/GCE (a), the AuNFs/Ch/GCE (b) and the ultralow Pt-loading AuNFs/Ch/GCE (c). Inset: enlarged *i*–*t* signals between 60 and 200 s. (B) Plots of chronoamperometric current versus H_2O_2 concentration for the Ch/GCE (a), the AuNFs/Ch/GCE (b) and the ultralow Pt-loading AuNFs/Ch/GCE (c). Inset: enlarged plots for H_2O_2 concentration ranges of 0.025–3.45 μM.

(curve (b)) and ultralow Pt-loading AuNFs/Ch/GCE (curve (c)) for the successive addition of certain concentrations of H_2O_2 into stirred PBS (pH 7.0) at an applied potential of 0.09 V. As expected from figure 5, the ultralow Pt-loading AuNFs/Ch/GCE exhibits a much larger catalytic current in response to a change of H_2O_2 concentration than those from the Ch/GCE and AuNFs/Ch/GCE. Figure 6(B) shows the calibration curve of H_2O_2 at the ultralow Pt-loading AuNFs/Ch/GCE (curve (a)). It can be seen that at a relatively low concentration (from 0.025 to 3.45 μM, the linear regression equation is $I(\mu A) = -4.077–3.184C$ (μM) and $R^2 = 9947$; figure 6(B), inset), the calibration plot is steeper than that at high concentration (from 5.91 to 94.3 μM, the linear regression equation is $I(\mu A) = -14.505–0.316C$ (μM) and $R^2 = 9989$), indicating that the ultralow Pt-loading AuNFs/Ch/GCE is more sensitive to H_2O_2 at low concentration. The detection limit of the H_2O_2 was 0.006 μM for a signal-to-noise ratio of 3. This result illustrates that the detection limit is much better than those of most enzyme-based H_2O_2 sensors [58–61] and

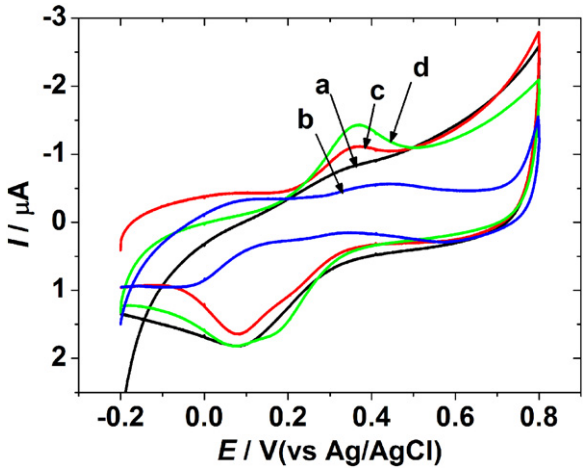

Figure 7. CVs of a AuNFs/Ch/GCE (b) and an ultralow Pt-loading AuNFs/Ch/GCE ((a), (c), (d)) in the absence of glucose (a) and in the presence of glucose with a concentration of 50 μM ((b), (c)) or 0.5 mM (d) in 0.1 M PBS (pH 7.0). Scan rate: 50 mV s^{-1}.

nanomaterial-based H_2O_2 sensors [62–64]. In particular, the ultralow Pt-loading AuNFs/Ch/GCE exhibited much better electrocatalytic activity towards the reduction of H_2O_2 than that of the bulk Pt@Au nanoparticle modified electrode [18, 65–67], and the results are listed in table S1 in the supporting information (available at stacks.iop.org/Nano/24/025501/mmedia).

3.4. Electrochemical performance of the ultralow Pt-loading AuNFs for glucose sensing

As shown in figure 7, the electrochemical performance for the oxidation of glucose at the ultralow Pt-loading AuNFs/Ch/GCE (curves (a), (c) and (d)) and the AuNFs/Ch/GCE (curve (b)) for comparison was investigated with CV measurements. From the CV scan of the AuNFs/Ch/GCE (curve (b)), it can be seen that a weak peak appears at ~0.01 V, which is due to the oxidation of glucose to gluconolactone and release of one proton per glucose molecule [68–71]. When the potential scans positively, the formation of AuOH sites increases on the electrode surface, which can catalyze the oxidation of gluconolactone into gluconate product [72–75]. Finally, free Au active sites are released for the direct oxidation of glucose, and it can be observed that the anodic current increases and a peak appears at ~0.44 V. For the ultralow Pt-loading AuNFs/Ch/GCE (curves (c) and (d)), only one well-defined peak for glucose oxidation can be observed at ~0.35 V (versus Ag/AgCl) and the first peak observed for the AuNFs/Ch/GCE disappears. This phenomenon is totally different from the results of direct glucose oxidation from Pt-based electrodes [68, 72, 76], which undergo three steps, including intermediate formation due to electrosorption of glucose, intermediate oxidation by Pt–OH and direct oxidation of glucose. We think that the glucose could be oxidized on the surface of the ultralow Pt-loading AuNFs, and thus just one peak could be found. Moreover, the anodic peak current value from the ultralow

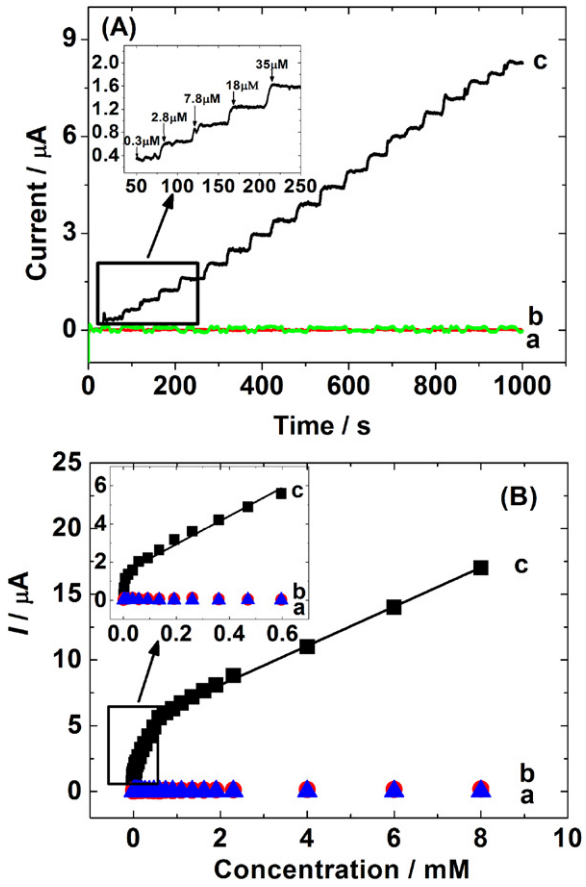

Figure 8. (A) Typical current–time response curves for the successive addition of a certain amount of glucose into stirred PBS (pH 7.0) at an applied potential of 0.4 V by the use of the Ch/GCE (a), the AuNFs/Ch/GCE (b) and the ultralow Pt-loading AuNFs/Ch/GCE (c). Inset: enlarged plots for the initial 250 s. (B) Plots of chronoamperometric current versus glucose concentration at the Ch/GCE (a), AuNFs/Ch/GCE (b) and ultralow Pt-loading AuNFs/Ch/GCE (c). Inset: linear calibration curves with a glucose concentration range of 0.0028–0.6 mM.

Pt-loading AuNFs/Ch/GCE at ~0.35 V is much larger than that from the AuNFs/Ch/GCE (~3.8 times). Such an improvement in glucose oxidation, including reaction pathway change and peak current increase, at the ultralow Pt-loading AuNFs/Ch/GCE compared with the Ch/GCE and AuNFs/Ch/GCE shows that the Pt monolayer on the surface of the AuNFs can greatly affect the catalytic properties of nanomaterials.

Figure 8(A) illustrates typical steady-state current–time curves for detecting glucose obtained using the Ch/GCE (a), AuNFs/Ch/GCE (b) and ultralow Pt-loading AuNFs/Ch/GCE (c) in 0.1 M PBS at a fixed potential of 0.4 V. Glucose was added at the points indicated by the arrows to the concentration stated (see inset). It can be observed that the ultralow Pt-loading AuNFs/Ch/GCE responds sensitively to the addition of glucose, which results from the excellent electrocatalytic activity towards glucose oxidation of the ultralow Pt monolayer. In comparison, the signal from the Ch/GCE and AuNFs/Ch/GCE is pretty weak. The calibration curve for the electrochemical response of the

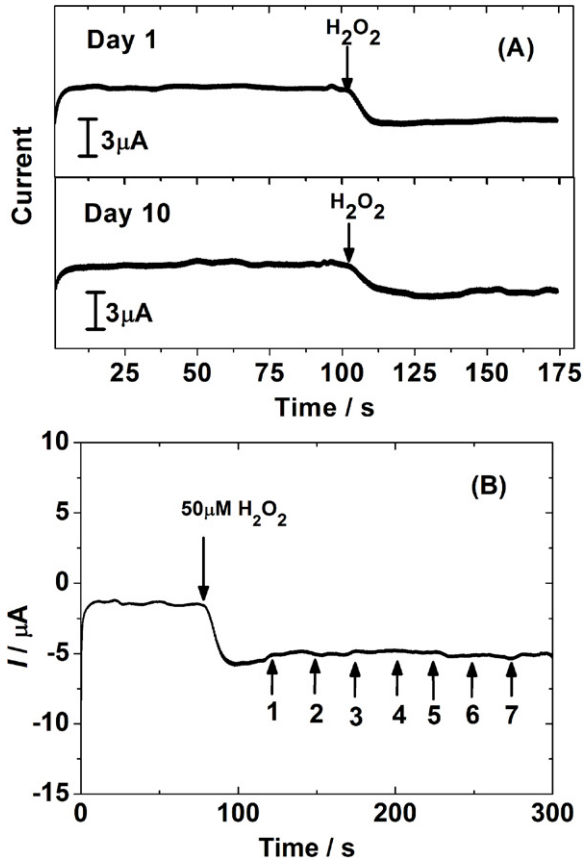

Figure 9. The amperometric response of the ultralow Pt-loading AuNFs/Ch/GCE for the detection of (A) 50 μM H_2O_2 at days 1 and 10, and (B) 50 μM H_2O_2 in the presence of 0.1 mM ascorbic acid (1), ethanol (2) , acetic acid (3), L-lysine (4), L-alanine (5), glycine (6) and uric acid (7).

electrode to glucose at 0.4 V can be obtained, as shown in figure 8(B). It can be seen that there exists a linear relationship in the concentration range of 0.0028–8.0 mM (linear equation of $I(\mu A) = 5.17 + 1.48C$ (mM), $R^2 = 0.9947$ for 0.6–8.0 mM; $I(\mu A) = 1.46 + 7.42C$ (mM), $R^2 = 0.9912$ for 0.0028–0.6 mM) with a detection limit of 0.8 μM. This detection limit is much lower than those obtained from other modified electrodes [4, 5, 10, 12, 14], especially bulk Pt–Au nanoparticle modified electrodes (shown in table S2 in the supporting information available at stacks.iop.org/Nano/24/025501/mmedia) [77, 78], indicating that this modified electrode can potentially be used as a glucose biosensor.

It must be pointed out that chloride ions in solution can be strongly adsorbed on a bare Au/Pt surface and the electrooxidation of glucose can be inhibited, which has been reported previously [75, 79–81]. This issue should be addressed if glucose sensing is applied in physiological conditions, although the buffer solution in our system is phosphate buffer solution (PBS). However, some results have shown that nanostructured Au surfaces, especially nanostructured Pt@Au surfaces, exhibit high resistance to deactivation by chloride ions during glucose electrooxidation [82–85]. We think that this ultrathin Pt coated AuNFs modified electrode may have good resistance to chloride ion blocking during glucose sensing and this work is in progress in our laboratory.

The stability and selectivity of the ultralow Pt-loading AuNFs biosensor were investigated. The stability of the biosensor was studied by chronoamperometric measurements in the presence of 50 μM H_2O_2 periodically (see figure 9(A)). When not in use, the biosensor was stored under high humidity (relative humidity, RH > 90%) at 25 °C. From figure 9(A), it can be observed that the biosensor only lost ~4% of its initial response after 10 days. For the selectivity test, some compounds that usually co-exist with glucose in human blood were investigated by the detection of 50 μM H_2O_2 with the successive addition of 0.1 mM ascorbic acid, ethanol, acetic acid, L-lysine, L-alanine, glycine and uric acid (see figure 9(B)). The result shows that the response signals from the above species are negligible and the anti-interference ability of this biosensor is good.

4. Conclusions

In this work, ultralow Pt-loading AuNFs were prepared by the underpotential deposition (UPD) monolayer redox replacement technique. The ultralow Pt-loading AuNFs exhibited high electrocatalytic activity, stability and selectivity towards hydrogen peroxide reduction and glucose oxidation. The high catalytic activity is due to the ultralow Pt monolayer, which can change the reaction pathway of glucose oxidation. This finding is of significance for the sensing application of bimetallic nanomaterials prepared by the UPD redox replacement technique, although they have been extensively investigated in fuel cells.

Acknowledgments

This work is financially supported by the National Natural Science Foundation of China (No. 20975002), the Key Project of the Chinese Ministry of Education and the Natural Science Research Project of the Education Department of Anhui Province (No. KJ2012A267).

References

[1] Safavi A and Farjami F 2011 *Biosens. Bioelectron.* **26** 2547–52
[2] Li D, Song S P and Fan C H 2010 *Acc. Chem. Res.* **43** 631–41
[3] Guo S J and Dong S J 2009 *Trac-Trends Anal. Chem.* **28** 96–109
[4] Chen K J, Lee C F, Rick J, Wang S H, Liu C C and Hwang B J 2012 *Biosens. Bioelectron.* **33** 75–81
[5] Xiao F, Zhao F Q, Mei D P, Mo Z R and Zeng B Z 2009 *Biosens. Bioelectron.* **24** 3481–6
[6] Jena B K and Raj C R 2011 *Biosens. Bioelectron.* **26** 2960–6
[7] Chaniotakis N and Sofikiti N 2008 *Anal. Chim. Acta* **615** 1–9
[8] Dodevska T, Horozova E and Dimcheva N 2006 *Anal. Bioanal. Chem.* **386** 1413–8
[9] Hrapovic S, Liu Y L, Male K B and Luong J H T 2004 *Anal. Chem.* **76** 1083–8
[10] Kang Q, Yang L X and Cai Q Y 2008 *Bioelectrochemistry* **74** 62–5
[11] Myung Y, Jang D M, Cho Y J, Kim H S, Park J, Kim J U, Choi Y and Lee C J 2009 *J. Phys. Chem.* C **113** 1251–9

[12] Wang H C, Wang X S, Zhang X Q, Qin X, Zhao Z X, Miao Z Y, Huang N and Chen Q 2009 *Biosens. Bioelectron.* **25** 142–6
[13] Wen D, Guo S J, Wang Y Z and Dong S J 2010 *Langmuir* **26** 11401–6
[14] Xu C X, Liu Y Q, Su F, Liu A H and Qiu H J 2011 *Biosens. Bioelectron.* **27** 160–6
[15] Hamm G, Becker C and Henry C R 2006 *Nanotechnology* **17** 1943–7
[16] Peng Z and Yang H 2009 *J. Am. Chem. Soc.* **131** 7542
[17] Jin Y, Shen Y and Dong S 2004 *J. Phys. Chem.* B **108** 8142–7
[18] Wang X L, Yang T, Feng Y Y, Jiao K and Li G C 2009 *Electroanal.* **21** 819–25
[19] Xing Y C, Cai Y, Vukmirovic M B, Zhou W P, Karan H, Wang J X and Adzic R R 2010 *J. Phys. Chem. Lett.* **1** 3238–42
[20] Koenigsmann C, Santulli A C, Gong K, Vukmirovic M B, Zhou W P, Sutter E, Wong S S and Adzic R R 2011 *J. Am. Chem. Soc.* **133** 9783–95
[21] Zhou W P, Sasaki K, Su D, Zhu Y M, Wang J X and Adzic R R 2010 *J. Phys. Chem.* C **114** 8950–7
[22] Wang J X, Ocko B M and Adzic R R 2003 *Surf. Sci.* **540** 230–6
[23] Carino E V, Kim H Y, Henkelman G and Crooks R M 2012 *J. Am. Chem. Soc.* **134** 4153–62
[24] Yancey D F, Carino E V and Crooks R M 2010 *J. Am. Chem. Soc.* **132** 10988–9
[25] Brankovic S R, Wang J X and Adžić R R 2001 *Surf. Sci.* **474** L173–9
[26] Gokcen D, Bae S-E and Brankovic S R 2010 *J. Electrochem. Soc.* **157** D582–7
[27] Gokcen D, Bae S-E and Brankovic S R 2011 *Electrochim. Acta* **56** 5545–53
[28] Bae S-E, Gokcen D, Liu P, Mohammadi P and Brankovic S 2012 *Electrocatal* **3** 1–8
[29] Brankovic S R, Vasiljevic N and Dimitrov N 2010 *Applications to Magnetic Recording and Microelectronic Technologies* (*Modern Electroplating*) ed M Paunovic and M Schlesinger (New York: Wiley)
[30] Fayette M, Liu Y, Bertrand D, Nutariya J, Vasiljevic N and Dimitrov N 2011 *Langmuir* **27** 5650–8
[31] Xu D, Bliznakov S, Liu Z, Fang J and Dimitrov N 2010 *Angew. Chem. Int. Edn* **49** 1282–5
[32] Liu Y, Bliznakov S and Dimitrov N 2009 *J. Phys. Chem.* C **113** 12362–72
[33] Sheridan L B, Czerwiniski J, Jayaraju N, Gebregziabiher D K, Stickney J L, Robinson D B and Soriaga M P 2012 *Electrocatal.* **3** 96–107
[34] Kim Y-G, Kim J Y, Vairavapandian D and Stickney J L 2006 *J. Phys. Chem.* B **110** 17998–8006
[35] Thambidurai C, Kim Y-G and Stickney J L 2008 *Electrochim. Acta* **53** 6157–64
[36] Carino E V and Crooks R M 2011 *Langmuir* **27** 4227–35
[37] Nakamura N, Sato N, Hoshi N and Sakata O 2010 *Langmuir* **26** 4590–3
[38] Wang Y X and Balbuena P B 2005 *J. Chem. Theory Comput.* **1** 935–43
[39] Panchenko A, Koper M T M, Shubina T E, Mitchell S J and Roduner E 2004 *J. Electrochem. Soc.* **151** A2016–27
[40] Chakraborty S and Raj C R 2009 *Biosens. Bioelectron.* **24** 3264–8
[41] Shin C, Shin W and Hong H G 2007 *Electrochim. Acta* **53** 720–8
[42] Gooding J J, Praig V G and Hall E A H 1998 *Anal. Chem.* **70** 2396–402
[43] Lee Y J, Park J Y, Kim Y and Ko J W 2011 *Curr. Appl. Phys.* **11** 211–6
[44] Kang X H, Mai Z B, Zou X Y, Cai P X and Mo J Y 2008 *Talanta* **74** 879–86
[45] Wang P, Mai Z B, Dai Z, Li Y X and Zou X Y 2009 *Biosens. Bioelectron.* **24** 3242–7
[46] Li Y X, Lin X Q and Jiang C M 2006 *Electroanalysis* **18** 2085–91
[47] Deinhammer R S, Ho M, Anderegg J W and Porter M D 1994 *Langmuir* **10** 1306–13
[48] Li Y X, Xian H Y and Zhou Y 2011 *Appl. Catal.* A **401** 226–32
[49] Li Y X, Wu S N, Chen Y L, Lu Q F and Wang L 2011 *Anal. Methods* **3** 1399–404
[50] Li Y X, Cox J T and Zhang B 2010 *J. Am. Chem. Soc.* **132** 3047–54
[51] Zhan D P, Velmurugan J and Mirkin M V 2009 *J. Am. Chem. Soc.* **131** 14756–60
[52] Qian L and Yang X 2006 *J. Phys. Chem.* B **110** 16672–8
[53] Jena B K and Raj C R 2008 *Anal. Chem.* **80** 4836–44
[54] *NIST X-ray Photoelectron Spectroscopy Database* 2003
[55] Li P W Y, Wang L and Lin X 2007 *Biosens. Bioelectron.* **22** 3120
[56] Shen J H, Yang X L, Zhu Y H, Kang H G, Cao H M and Li C Z 2012 *Biosens. Bioelectron.* **34** 132–6
[57] Kristian N, Yan Y and Wang X 2008 *Chem. Commun.* 353–5
[58] Liu Y, Lei J and Ju H 2008 *Talanta* **74** 965
[59] Lu D, Kordiel J, Cao G and Shen A Q 2010 *Adv. Mater.* **22** 2809–13
[60] Wang J, Wang L, Di J and Tu Y 2009 *Talanta* **77** 1454–9
[61] Liu Y L, Yang Y H, Yang H F, Liu Z M, Shen G L and Yu R Q 2005 *J. Inorg. Biochem.* **99** 2046–53
[62] Fang Y G, Zhu S, Zhai C, Wang Y and E 2010 *Langmuir* **26** 11277–82
[63] Bian X L, Jin X, Kong E, Zhang L, Wang W and C 2010 *Talanta* **81** 813–8
[64] Li Y Z, Xuan J, Jiang J and Zhu L 2010 *J. Electrochem. Commun.* **12** 777–80
[65] Zhang Y, Yuan R, Chai Y Q, Wang J F and Zhong H A 2012 *J. Chem. Technol. Biotechnol.* **87** 570–4
[66] Kang X H, Mai Z B, Zou X Y, Cai P X and Mo J Y 2007 *Anal. Biochem.* **369** 71–9
[67] Li J P, Yu J G, Wei X P and Liu R 2011 *J. Solid State Electrochem.* **15** 1129–37
[68] Yuan J, Wang K and Xia X 2005 *Adv. Funct. Mater.* **15** 803–8
[69] Vassilyev Y B, Khazova O A and Nikolaeva N N 1985 *J. Electroanal. Chem.* **196** 105–25
[70] Lei H W, Wu B L, Cha C S and Kita H 1995 *J. Electroanal. Chem.* **382** 103–10
[71] Larew L A and Johnson D C 1989 *J. Electroanal. Chem.* **262** 167–82
[72] Prehn R, Cortina-Puig M and Muñoza F X 2012 *J. Electrochem. Soc.* **159** F134–9
[73] Xia Y, Huang W, Zheng J, Niu Z and Li Z 2011 *Biosens. Bioelectron.* 2 **6** 3555–61
[74] Adzic R R, Hsiao M W and Yeager E B 1989 *J. Electroanal. Chem. Interfacial Electrochem.* **260** 475–85
[75] Hsiao M W, Adzic R R and Yeager E B 1992 *Electrochim. Acta* **37** 357–63
[76] Wang J and Thomas D F 2008 *A. Chen. Anal. Chem.* **80** 997–1004
[77] Lee Y J and Park J Y 2011 *Sensors Actuators* B **155** 134–9
[78] Ryu J, Kim K, Kim H S, Hahn H T and Lashmore D 2010 *Biosens. Bioelectron.* **26** 602–7
[79] Hsiao M W, Adzic R R and Yeager E B 1996 *J. Electrochem. Soc.* **143** 759–67
[80] Li Y, Song Y-Y, Yang C and Xia X-H 2007 *Electrochem. Commun.* **9** 981–8
[81] Cho S, Shin H and Kang C 2006 *Electrochim. Acta* **51** 3781–6
[82] Seo B and Kim J 2010 *Electroanal.* **22** 939–45
[83] Jeong H and Kim J 2012 *Electrochim. Acta* **80** 383–9
[84] Qiu H and Huang X 2010 *J. Electroanal. Chem.* **643** 39–45
[85] Seo B, Choi S and Kim J 2011 *ACS Appl. Mater. Interfaces* **3** 441–6